Spatial changes in the summer diatom community of the northern Bering Sea in 2017 and 2018

Yuri Fukai[a,*,†], Yoshiyuki Abe[b,c], Kohei Matsuno[a,d], Atsushi Yamaguchi[a,d]

[a]*Faculty/Graduate School of Fisheries Sciences, Hokkaido University, 3−1−1 Minato-cho, Hakodate, Hokkaido 041-8611, Japan*

[b]*Atmosphere and Ocean Research Institute, The University of Tokyo, 5-1-5, Kashiwanoha, Kashiwa-shi, Chiba, 277-8564, Japan*

[c]*Research Development Section, Office for Enhancing Institutional Capacity, Hokkaido University, Kita 21, Nishi 10, Kita-ku, Sapporo, Hokkaido, 001-0021, Japan*

[d]*Arctic Research Center, Hokkaido University, Kita-21 Nishi-11 Kita-ku, Sapporo, Hokkaido, 001-0021, Japan*

† Present address: *Division of Earth System Science, Graduate School of Environmental Science, Hokkaido University, Kita-10 Nishi-5 Kita-ku, Sapporo, Hokkaido, 060-0810, Japan*

* Corresponding author, Tel: 81-11-706-2246, Fax: 81-11-706-2247

E-mail address: fukai@ees.hokudai.ac.jp (Y. Fukai)

ABSTRACT

In recent years, the northern Bering Sea has experienced changes in the timing of sea-ice retreat and in hydrographic conditions during the summer. The influence of these environmental changes on the diatom community has not been examined. In this study,

we investigated the spatial changes in the diatom community of the northern Bering Sea during the summers of 2017 and 2018, and evaluated the effects of environmental variability on these communities. We found that the diatom cell density and diversity varied with water masses. A cluster analysis based on cell density revealed that the diatom communities were separated into four groups, and that the distributions of three of these groups were different spatially between 2017 and 2018. In the Bering Strait and the Chirikov Basin regions, the diatom communities differed between 2017 and 2018. In 2017, these diatom communities were dominated by cold-water species such as *Chaetoceros gelidus* and *Chaetoceros* spp. (subgenus *Hyalochaetae*), while in 2018, the community was dominated by cosmopolitan species such as *Thalassionema nitzschioides* and *Chaetoceros* spp. (subgenus *Phaeoceros*). NMDS and multiple regression analysis indicated that the timing of the sea-ice retreat was the most important contributor to the differences in the diatom community. In contrast, there was no year-to-year difference south of St. Lawrence Island, possibly because nutrients were depleted and phytoplankton types other than diatoms were dominant.

Keywords: Northern Bering Sea, Phytoplankton community, Diatoms, Year-to-year changes

1. Introduction

The northern Bering Sea is one of the most productive ocean regions in the world (Springer and McRoy, 1993). Supported by the high primary production, the area is important for higher trophic level species such as sea birds and marine mammals (Springer et al., 1996). This region is now facing drastic changes in sea-ice cover and hydrographic conditions during summer (Grebmeier et al., 2015; Frey et al., 2018). For example, reduced sea-ice cover in 2018 resulted in a diminished deep cold pool (< 2 °C) south of St. Lawrence Island, and groundfish from the southeastern Bering Sea shifted northward., while the abundance of arctic species decreased in the region (Cornwall, 2019; Duffy-Anderson et al., 2019). Given that sea-ice reduction is known to have affected some components of the northern Bering Sea, investigation of other components is required to understand the effects of future changes (Huntington et al., 2020).

The northern Bering Sea is a shallow shelf region. This region has a complicated hydrographic environment due to the inflow of multiple currents with different hydrographic features. The mixing of these waters results in complex hydrographic environments that affect the distribution of phytoplankton communities (Giesbrecht et al., 2019). In the northern Bering Sea, phytoplankton supports a high level of primary production in the upper mixed layer; most of this production settles to the seafloor due to low zooplankton grazing pressure (Grebmeier et al., 1988).

Diatoms play an important role as primary producers in high latitude marine ecosystems. A large diatom bloom occurs in the northern Bering Sea from the late spring to early summer, when the sea ice is melting and the light limit is diminishing; the chlorophyll *a* concentration can exceed 8 μg L^{-1} during these blooms (Springer and McRoy, 1993). During the spring Arctic bloom, *Chaetoceros gelidus* sometimes

dominates (von Quillfeldt, 2000; Sergeeva et al., 2010). The composition of diatom communities varies among the different hydrographic environments (Taniguchi et al., 1976; Sergeeva et al., 2010). Diatoms constitute an important taxon in this marine ecosystem and require evaluation to understand how they respond to environmental change.

From 1978 to 2012, the timing of the sea-ice retreat (TSR) south of St. Lawrence Island, in the Chirikov Basin and in the Chukchi Sea has become earlier (Grebmeier et al., 2015; Frey et al., 2018). In the northern Bering Sea, the magnitude and timing of the phytoplankton bloom varies with the timing of the spring sea - retreat (Fujiwara et al., 2016). In 2018, the TSR was approximately two weeks earlier than it was during the previous year; the magnitude of the ice algal bloom was small and zooplankton abundance decreased (Cornwall, 2019; Fukai et al., 2019). However, despite the importance of diatoms for primary production, there is no information on how the diatom community responds to changes in sea-ice dynamics in the northern Bering Sea.

The purpose of our paper is to examine the phytoplankton communities, particularly with a focus on the diatom communities of the northern Bering Sea from 62°N to the Bering Strait. To this end, we describe the species composition of diatoms, and test three hypotheses: 1) that the cell density and species composition of the diatom community differ by water mass, 2) that the diatom community differed between 2017 and 2018, and 3) that the hydrography, including sea-ice condition before sampling, will affect the diatom community.

2. Materials and methods

94 *2.1. Study area*

95

96 Sampling was conducted along the northern Bering Sea shelf from July 9–21,
97 2017 and July 2–12, 2018 during the 40th and 56th cruises, respectively, of the *T/S*
98 *Oshoro-Maru* of Hokkaido University (Fig. 1). The study areas were the waters south of
99 St. Lawrence Island, the Chirikov Basin (from the north of St. Lawrence Island to the
100 south of Bering Strait), and the Bering Strait.

101

102 *2.2. Sea Ice*

103

104 Data on sea ice concentration (SIC) were obtained from the Advanced
105 Microwave Scanning Radiometer 2 (AMSR2) to evaluate the extent of the sea ice. These
106 AMSR2 data were supplied by the Japan Aerospace Exploration Agency via the Arctic
107 Data archive System (ADS) (https://ads.nipr.ac.jp/), through the cooperation of the
108 National Institute of Polar Research and JAXA. We used the SIC data after calculating a
109 5-day moving average. Sea-ice covered regions were defined as having a SIC > 20%. In
110 addition, the TSR was defined as the last date when the SIC was at 20% prior to the
111 observed annual sea ice minimum across the study region.

112

113 *2.3. Physical Oceanography*

114

115 Conductivity-temperature-depth (CTD) casts were conducted at 40 stations in
116 2017 and 28 stations in 2018 to obtain vertical profiles of the temperature, salinity, and
117 chlorophyll *a* fluorescence (see Appendix Fig. 1). We used a CTD (SBE911, Sea-Bird
118 Electronics, Inc.) calibrated prior to the cruise. The mixed-layer depth was defined as the

depth where density was 0.10 kg m^3 greater than the value at 5 m depth (Danielson et al., 2011).

2.4. Nutrients

At 26 of the CTD stations (14 stations in 2017 and 12 stations in 2018), water samples for nutrient analysis were collected from 4–6 layers every 10 m from the surface to 5 m above the seafloor using a bucket and Niskin bottles (Fig. 1). The obtained unfiltered nutrient samples (n = 128) in Spitz tubes were frozen on board at -80 °C. In the shore-based laboratory, the major nutrients (NO_2-N + NO_3-N, NH_4-N, PO_4-P, and Si $(OH)_4$) were measured by colorimetric methods using a QuAAtro 2-HR system certified with standard reference materials for nutrient analysis (KANSO, standard Lot BT, BZ, Osaka, Japan) in accordance with "The GO-SHIP Repeat Hydrography Manual" (Hydes et al., 2010).

2.5. Phytoplankton

Water samples for phytoplankton counts were collected from the same stations and layers as the nutrient samples. A total of 141 phytoplankton samples was collected and preserved as follows: in 2017, 500 mL water samples were concentrated 50-fold using a nucleopore filter (3.0 μm) before being preserved with glutaraldehyde at a final concentration of 1%. Note that the diatoms and dinoflagellates addressed in this study experience little damage from filtering (Dahl and Naustvoll, 2010). In 2018, 1 L of each water sample was preserved on board with glutaraldehyde at a final concentration of 1%. The samples were then settled and concentrated 24- to 33- fold using siphon tubes in the

144 land laboratory.

145 Aliquots (1 mL) of the concentrated samples were transferred to a glass slide to
146 count and identify the diatoms and dinoflagellates with an inverted microscope at 200–
147 600 × magnification. The diatoms and dinoflagellates were counted and identified from
148 approximately 300 cells. When the cell number count was less than 300 cells, the
149 minimum numbers were 18 cells in 2017 and 21 cells in 2018. In addition, the detection
150 limits were 20 cells L^{-1} in 2017 and 30 cells L^{-1} in 2018, suggesting that there was not
151 much difference (ability to detect low numbers of cells in a sample) between the years.
152 As explained in Hasle and Syvertsen (1997) and Hoppenrath et al. (2009), the diatoms
153 were identified to the species or genus level and the dinoflagellates were identified to the
154 genus level. Distinguishing *Cylindrotheca closterium* from *Nitzschia longissima* was
155 difficult (Hasle and Syvertsen, 1997), so these species were treated as *Cy. closterium*. In
156 addition, *C. convolutus*, *C. concavicornis* and *C. borealis* were nearly indistinguishable
157 because they were damaged by current transportation, as mentioned by Taniguchi et al.
158 (1976), so they were collectively counted and identified as *C.*
159 *convolutus/concavicornis/borealis*.

160 Using the counting data, the diversity of diatoms was evaluated by Shannon-
161 Wiener index (*H'*).

162 $$H' = -\sum \frac{n}{Ni} \times \ln \frac{n}{Ni}$$

163 where *n* is the cell density (cells mL^{-1}) of *i*th species and *Ni* is the total diatom cell density
164 (cells mL^{-1}) at each station (Shannon and Weaver, 1949).

165

166 *2.6. Statistical analyses*

167

168 Differences in phytoplankton cell density among the water masses in the upper

169 mixed-layer was tested by Mann-Whitney U-test. For comparison of the diatom
170 community among the water masses, we performed cluster analyses, nonmetric
171 multidimensional scaling (NMDS) ordinations, and multiple regression analyses for each
172 year or with each water mass, but the results could not be interpreted (cf. Appendix Figs.
173 2, 3). Also, to compare the diatom diversity (*H'*) among the water masses, a one-way
174 analysis of variance (ANOVA) was used. If the ANOVA identified statistically significant
175 differences ($p < 0.05$), a post hoc Tukey-Kramer test was used to clarify the interactions
176 among the water masses.

177 Differences between the years of the NO_2-N + NO_3-N concentration, which was
178 likely to be a limiting factor among nutrients, were compared by a Mann-Whitney U-test
179 for each region. Similarly, differences of the phytoplankton cell density between 2017
180 and 2018 in the Bering Strait, and of diatom diversity (*H'*) between 2017 and 2018 were
181 tested using a Mann-Whitney U-test.

182 To compare the diatom community between 2017 and 2018, we first performed
183 a cluster analysis based on the cell density within each water mass (Appendix Fig. 2).
184 Several patterns of the cluster analysis were tested in each year, by water mass, and by
185 depth (cf. Appendix Figs. 2, 3). The results of these tests were uninterpretable, so we used
186 analyses based on all diatom samples from a given year. Thus, this analysis focused on
187 describing year-to-year changes in the diatom community (species composition) between
188 2017 and 2018. To reduce the bias for abundant species, the cell density data (X: cells
189 mL^{-1}) for each species were transformed to $\sqrt[4]{X}$ prior to cluster analysis (Quinn and
190 Keough, 2002). The similarities between samples were examined using the Bray-Curtis
191 index based on the differences in the species composition. To group the samples, the
192 similarity indices were coupled using hierarchical agglomerative clustering with a
193 complete linkage method (an unweighted pair group method using the arithmetic mean)

(Field et al., 1982).

To delineate the sample groups on a two-dimensional map, NMDS ordination was conducted. Thereafter, multiple regression analyses (Y = aX1+ bX2+c, where Y is the environmental variable and X1 and X2 are axes 1 and 2 of NMDS, respectively) were performed to clarify which environmental variables (temperature, salinity, chlorophyll *a* fluorescence, concentrations of NO_2-N + NO_3-N, NH_4-N, dissolved inorganic nitrogen (DIN), PO_4-P, and Si $(OH)_4$, the ratio of the DIN concentration to that of PO_4-P (N:P ratio), the timing of the sea-ice retreat (TSR), observation date, and sampling depth) had significant relationships with the phytoplankton groups.

Furthermore, to test intergroup differences in the diatom cell density and hydrographic environments (temperature, salinity, chlorophyll *a* fluorescence, concentrations of NO_2-N + NO_3-N, NH_4-N, DIN, PO_4-P, and Si $(OH)_4$, the N:P ratio, and the TSR), a one-way ANOVA and a post hoc Tukey-Kramer test were used. All the analyses were conducted with PRIMER 7 (PRIMER-E Ltd.) or Stat View v5 (SAS Institute Inc.).

3. Results

3.1. Sea Ice

In 2017, the study region south of St. Lawrence Is. was first completely ice-covered on January 19, and in 2018, sea-ice cover was not complete until February 5. The sea ice first covered the Bering Strait and the Chirikov Basin, except for the most eastern station, on January 11, 2017 and December 28, 2018. In some stations in 2018 (St. 11 and

St. 14), the SIC was repeatedly over and below 20%. In the most eastern stations in the Chirikov Basin (St. 5 in 2017 and St. 19 in 2018), the SIC exceeded 20% on December 8, 2016 and 2017.

South of St Lawrence Island, in 2017, sea ice was completely gone by May 3, whereas in 2018, ice left over a month earlier, on March 24. In 2017, the first day in the study area when the Chirikov Basin had an ice concentration < 20% was on April 5, whereas, in 2018, open water was first detected on March 25, 11 days earlier.

3.2. Hydrography and nutrient chemistry

We identified four water masses that differed in physical characteristics; Bering Chukchi Summer Water (BCSW) (moderate/cold with high salinity), Bering Chukchi Winter Water (BCWW) (cold with high salinity), Alaskan coastal water (ACW) (warm with low salinity), and Melting Water (MW) (cold with low salinity) (Danielson et al., 2017) (Figs. 2, 3). The water masses (> 12 °C in ACW and > 7 °C in BCSW) that were unidentified by Danielson et al. (2017) were defined as ACW or BCSW based on their salinity (Fig. 3).

In 2017, the BCWW (< 0 °C) was present at the bottom south of St. Lawrence Island (Fig. 4). The BCSW was present throughout the water column in the Bering Strait and the northern Chirikov Basin. By contrast, in the eastern coastal area and south of 65 °N in the Chirikov Basin, the ACW was present in the surface layer and the BCSW was observed in the lower layer (Fig. 4).

In 2018, the BCWW (< 0 °C) was not present at the bottom in the region South of St. Lawrence Island (Fig. 4). The BCSW was present throughout the water column in the Bering Strait and the Chirikov Basin, except for the eastern coastal area where the

ACW was observed in the surface layer (Fig. 4).

The distribution of water masses differed between the years. In 2017, ACW was present in the surface layer of the southwestern Chirikov Basin and there was BCSW at the bottom south of St. Lawrence Island; these were not present in 2018.

In both years south of St. Lawrence Island, fluorescence above the pycnocline (avg = 0.07 and 0.16 in 2017 and 2018, respectively) was lower than that below the pycnocline (avg = 0.39 and 0.60 in 2017 and 2018, respectively) (Fig. 5). In Bering Strait, fluorescence was similar in both years (2017, avg = 0.90: 2018, avg = 0.78) (Fig. 5). In the Chirikov Basin, fluorescence above the pycnocline was higher in 2017 (avg = 0.69) than in 2018 (avg = 0.26), while, below the pycnocline fluorescence was similar in both years (Fig. 5).

To the south of St. Lawrence Island, the NO_2-N + NO_3-N was depleted in the upper mixed layer in both years, but it was high below the pycnocline (Fig. 5) with no significant differences between the years (*U-test*, $p > 0.05$). In the Bering Strait, NO_2-N + NO_3-N did not differ significantly between years (*U-test*, $p > 0.05$) (Fig. 5). In this region, the lowest concentration of nitrate plus nitrite was at the eastern station (st. 5) in 2017, whereas in 2018, the highest concentrations were found in the northern Bering Strait (st. 29). In the Chirikov Basin, these nutrients were not significantly different between the years (*U-test*, $p > 0.05$); in both years, the lowest concentrations were detected at the eastern stations (st. 11 in 2017 and st. 19 in 2018).

Concentrations of other nutrients were generally similar between years at the same station. In both years in each region, NH_4-N concentrations were similar (Fig. 5). Likewise, the PO_4-P concentrations did not vary between years within regions; the highest value detected was in the Bering Strait in 2017 (st.1, 6.62 μM) (Fig. 5). We found high concentrations of Si $(OH)_4$ over major portions of the study region in both years, except

for some stations in 2018 in the eastern Chirikov Basin (st. 11 in 2018) and the south of St. Lawrence Island (sts. 4, 6, 8 in 2018), where this nutrient was not detectable (Fig. 5). In both years, the N:P ratio was below 16 throughout most of the study area.

3.3. Phytoplankton community

3.3.1. Cell density

In the upper mixed layer, the cell density of diatoms and dinoflagellates was significantly different in each water mass, and it was higher in BCSW than in ACW (*Mann-Whitney U-test*, $p < 0.05$), whereas, cell densities below the pycnocline did not differ among water masses (*one-way ANOVA*, $p > 0.05$). In both 2017 and 2018, the highest cell densities were observed in the Bering Strait (2017: 1.6×10^6 cells L^{-1} and in 2018: 3.4×10^5 cells $L^{-1)}$ with diatoms and dinoflagellates in this region more abundant in 2017 (stations 1–3) than in 2018 (stations 27–30) (*Mann-Whitney U-test*, $p < 0.05$) (Fig. 6).

3.3.2. Phytoplankton species and their diversity

A total of 29 genera and 30 species of diatoms (centric diatoms: 19 genera and 25 species and pennate diatoms: 10 genera and 5 species) and 6 genera and 5 species of dinoflagellate were observed over the two years (Table 1).

The diversity of the diatoms (*H'*) ranged from 0–3.56 in 2017 and 0.36–2.98 in 2018. The *H'* varied among water masses, with values significantly higher in BCWW and BCSW than in ACW (*one-way ANOVA*, $p < 0.05$). There were no significant differences in the diversity of diatoms between the years (*Mann-Whitney U-test*, $p > 0.05$).

294 *3.3.3. Phytoplankton community by cluster analysis*

295 Phytoplankton communities were classified into four groups (A–D) by a cluster
296 analysis at 27% and 37% similarity levels (Fig. 7a). Group A was low-density (1.3×10^3–
297 1.3×10^5 cells L^{-1}, avg = 4.6×10^4 cells L^{-1}) and was composed primarily of *C. gelidus*
298 (Fig. 7b). Group B had the highest cell density (1.6×10^3–1.6×10^6 cells L^{-1}, avg = $2.5 \times$
299 10^5 cells L^{-1}), and *Hyalochaetae* such as *C. gelidus*, *C. furcellatus*, and *C. debilis* were
300 dominant (64%) (Fig. 7b). The cell density of *C. gelidus*, *C. diadema*, and *Chaetoceros*
301 spp. in group B was significantly higher than it was in groups C and D. The cell density
302 of group C was nearly as low as it was in group A (3.3×10^3–1.2×10^5 cells L^{-1}, avg =
303 3.4×10^4 cells L^{-1}); however, the community composition was very different. *Phaeoceros*
304 such as *C. convolutus/concavicornis/borealis* had a relatively high density in group C
305 (13%), and the pennate diatoms such as *Thalassionema nitzschioides* and *Cylindrotheca*
306 *closterium* had a significantly higher density in group C than it did in the other groups
307 (Table 2). Group D had the lowest cell density (3.6×10^2–4.4×10^5 cells L^{-1}, mean $2.5 \times$
308 10^4 cells L^{-1}) and *Leptocylindrus* spp. dominated (85%).

309 The phytoplankton communities were different in each region (Fig. 7c). In both
310 years south of St. Lawrence Island, group D was present in the upper layer (0 m or 0–20
311 m) and groups A, B, and C occurred in the deeper layers. From 65°N (the Chirikov Basin)
312 to the Bering Strait, the distribution varied across years; group B was observed throughout
313 the area in 2017, but group C was observed in 2018. In these regions (the Chirikov Basin
314 and the Bering Strait), the spatial distribution of water masses and phytoplankton
315 community groups as determined by the cluster analysis did not match (Fig.4, Fig.7c),
316 thus, the groups were different between years even though BCSW was occupied in both
317 years.
318

3.3.4. Relationships between phytoplankton communities and environmental factors

On the NMDS ordination, phytoplankton plots had significant relationships with various environmental variables ($p < 0.05$), including chlorophyll *a* fluorescence (r^2 = 0.30), TSR ($r^2 = 0.28$), observation date ($r^2 = 0.16$), sampling depth ($r^2 = 0.13$), salinity ($r^2 = 0.11$), Si $(OH)_4$ ($r^2 = 0.08$) and NO_2+NO_3 ($r^2 = 0.05$) (Fig. 7d), but the other parameters did not. Especially note that temperature did not have a significant relationship with phytoplankton plots ($p > 0.05$), and that the contribution of TSR to diatom groups was the highest among environmental factors except for chlorophyll *a* fluorescence.

In addition, the one-way ANOVA and Tukey-Kramer test indicated that the PO_4 and DIN concentrations and the N:P ratio did not differ significantly among phytoplankton groups (*one-way ANOVA*, $p > 0.05$). However, the other hydrographic variables differed between groups B and D. Group D had a higher temperature and lower salinity, nutrients (NO_2+NO_3, PO_4-P, NH_4-N, Si $(OH)_4$), and chlorophyll *a* fluorescence than the other groups. Groups B and C differed only in their salinity, chlorophyll *a* fluorescence and TSR (Table 3). Especially note that temperature was not significantly different between Group B and C.

4. Discussion

4.1. The influence of water masses

Diatom community structure (i.e. species composition and their cell density) was not consistently correlated with water mass during summer except for the stations south of St. Lawrence Island. However, there were significant differences among the water

masses in the cell density in the upper mixed layer and in diatom diversity. These differences may have been related to differences in the nutrient content of the water masses. Differences in characteristics of water masses are known to influence phytoplankton cell density (Coachman et al., 1975; Danielson et al., 2017; Giesbrecht et al., 2019). The N:P ratio was below 16 throughout the study area, which indicated that the DIN was the limiting nutrient concentration, and differences in DIN concentrations in the various water masses was one of the most important factors for the growth of phytoplankton upper the mixed layer over the study area. Thus, phytoplankton cell density was higher in the upper mixed layer in the BCSW, including the nutrient-rich AW, than in the nutrient-poor ACW (Coachman et al., 1975; Danielson et al., 2017).

The diversity of diatoms indicated by *H'* was higher in BCWW and BCSW than in ACW in the same way as the DIN concentration was. We suggest that the differences in the diversity of diatoms between water masses was related to difference in nutrient concentrations between water masses, especially the DIN concentrations. As mentioned above, DIN was the limiting factor in the nutrient concentration and thus, in the water masses with high DIN such as BCWW and BCSW, competition for DIN may have been minimal, thus resulting in many diatom species surviving in these waters.

4.2. The phytoplankton community of the south of St. Lawrence Island

In contrast to the Chirikov Basin and the Bering Strait regions, south of St Lawrence Island year-to-year changes in the phytoplankton community were not observed. In the upper mixed layer south of St. Lawrence Island, nutrient-poor ACW was present in both years, and the DIN concentrations and, at some stations the Si $(OH)_4$ concentrations, were too low to support diatom growth (Justic et al., 1995). The lack of

DIN may have resulted in the dominance of phytoplankton group D, which was predominately non-diatom species that can thrive in low nutrient conditions (Parsons et al., 1978). The timing and magnitude of the spring phytoplankton bloom in the region south of St. Lawrence Island differed in 2017 and 2018, and we hypothesize that this was due to differences in the TSR (Fukai et al., 2019; Hirawake, per. comm.). Thus, after the nutrients were depleted from the upper mixed layer, phytoplankton, other than diatoms, dominated. A similar succession may occur in the eastern Bering Sea where coccolithophore blooms during the summer were reported after the diatom bloom (Stockwell et al., 2001; Iida et al., 2002). Coccolithophore blooms were also observed by satellite observation from the eastern Bering Sea to south of St. Lawrence Island after 2000s (Harada et al., 2012). In our study, it is not clear whether the phytoplankton community changed at the species level, because dinoflagellates and phytoplankton other than diatoms were not identified to the species level.

4.3. The changes in the summer diatom community in the Chirikov Basin and the Bering Strait, 2017-2018

From 65°N (the Chirikov Basin) to the Bering Strait, between 2017 and 2018, phytoplankton cell density declined and community structure changed. In this region in 2017, the highest cell density (1.6×10^6 cells L^{-1}) was nearly the same as that reported by Sergeeva et al. (2010) for July 2003 and by Giesbrecht et al. (2019) (the highest density was approximately 10^6 cells L^{-1}). In 2018, the highest cell density (3.4×10^5 cells L^{-1}) was only 34% of the values observed in 2017.

With respect to the phytoplankton community, in 2017, group B was widely distributed and had a high cell density that was dominated (64%) by *Hyalochaetae* such

as *C. gelidus* and *C. furcellatus*. *C. gelidus* and *C. furcellatus* are cold-water species and are common in the Arctic (Hasle and Syvertsen, 1997; Hoppenrath, 2009). These species are typically found in the Chukchi Sea adjacent to the study area (von Quillfeldt et al., 2003). In 2018, Group C, which was mostly composed of *Thalassionema nitzschioides*, was widely distributed. The abundance of *Chaetoceros* spp. was low (20%), and *Phaeoceros* such as *C. convolutus/concavicornis/borealis* made up most of the *Chaetoceros* spp. *T. nitzschioides* and *C. convolutus* are known as cosmopolitan species; the former does not occur in the high Arctic and the latter is common in temperate waters (Hasle and Syvertsen, 1997; Hoppenrath, 2009). *T. nitzschioides* has also been reported in temperate water after the melting of the sea ice (Neeley et al., 2018), and it is a characteristic species of the Pacific-Arctic region in the autumn (Matsuno et al., 2014). These results suggest that between 2017 and 2018, the summer diatom community in the Bering Strait and the Chirikov Basin changed from cold water to cosmopolitan species.

Interestingly, the NMDS, the multiple regressions, and the one-way ANOVA did not suggest any significant differences in temperature between 2017 and 2018 in the region north of 65°N. By contrast, the TSR was the most important contributing factor among the environmental factors for explaining the differences in the diatom communities between the two years. There was also a significant difference in the TSR between group B in 2017 and C in 2018. Because the TSR differed between 2017 and 2018 in the northern Bering Sea (Cornwall, 2019; Fukai et al., 2019; Grebmeier et al., 2019), the effect of the TSR on the summer diatom community cannot be ignored.

The TSR affects the magnitude and timing of the spring bloom in the seasonal sea ice area (Hunt et al., 2002; Fujiwara et al., 2016). The magnitude of the phytoplankton bloom in the open water is usually large when the TSR is early (Hunt et al., 2002; Fujiwara et al., 2016). In 2018, when the TSR was early, large increases in sea surface chlorophyll

419 *a* in the Chirikov Basin were observed with satellite remote sensing from early to late
420 May after the sea ice had completely retreated (Hirawake, per. comm.). Hence, in 2018,
421 when the TSR was early, the available nutrients may have been consumed by the large
422 open-water bloom during early spring after the sea ice retreat, resulting in the wide
423 distribution of phytoplankton community group C during summer, with a low cell density.
424 In summer 2018, the cosmopolitan species composition of group C, some of which, such
425 as *T. nitzschioides,* are species characteristic of the autumn (Matsuno et al., 2014), and
426 might been the result of the early TSR in 2018 and an early depletion of nutrients.
427
428
429 **5. Conclusions**
430
431 This study described and compared northern Bering Sea diatom communities in
432 the summers of 2017 and 2018. The diatom cell density and diatom diversity differed by
433 water mass. Year-to-year differences in the diatom community between 2017 and 2018
434 were found, depending on the region examined. South of St. Lawrence Island, we found
435 no changes in the diatom community between 2017 and 2018. Nitrate and nitrite were
436 depleted in the upper mixed layer in both years, and phytoplankton types other than
437 diatoms dominated this region. Since we focused our study on diatoms, it is possible that
438 there were interannual changes in other elements of the phytoplankton community that
439 we did not detect.
440 In the Chirikov Basin and Bering Strait, diatom communities in 2017 and 2018
441 differed, even though the same water masses were present in both years. The TSR was
442 much earlier in 2018 than in 2017, though summer water temperatures were similar in the
443 two years. Since nutrient concentrations were lower in 2018, we hypothesize that the open

water bloom in 2018 may have depleted the nutrients, with the result that in 2018 several sub-arctic or cosmopolitan species were abundant compared to 2017, when arctic species predominated. It will be important to evaluate the influence of the changing diatom community on the marine ecosystem of the northern Bering and Chukchi Seas. To this end, focus on the entire phytoplankton community, including dinoflagellates, coccolithophores and others, will be required.

Acknowledgments

We thank the captain, officers, crew, and researchers on board the *T/S Oshoro-Maru*, of Hokkaido University, for their contributions during field sampling. We thank Toru Hirawake, chief scientist of the cruises. We also thank two anonymous reviewers for their helpful comments. This study was conducted by the Arctic Challenge for Sustainability (ArCS) project and Arctic Challenge for Sustainability II (ArCS II) project. The ADS dataset is archived and was provided by the Arctic Data archive System (ADS), which was developed by the National Institute of Polar Research. Part of this study was supported through Grants-in-Aid for Scientific Research 17H01483 (A), 19H03037 (B), 20H03054 (B), 18K14506 (Early-Career Scientists) and 20K20573 (Challenging Research (Pioneering)) from the Japan Society for the Promotion of Science.

References

Coachman, L.K., Aagaard, K., Tripp, R.B., 1975. Bering Strait: The regional physical oceanography. University of Washington Press, Seattle, WA.

Cornwall, W., 2019. Vanishing Bering Sea ice poses climate puzzle for second winter in a row, ice cover shrinks to lowest levels seen in at least 4 decades. Science 364, 616–617.

Dahl, E., Naustvoll, L.J., 2010. Filtering – semitransparent filters for quantitative phytoplankton analysis. In: Karlson, B., Cusack, C., Bresnan, E. (Eds.). Microscopic and molecular methods for quantitative phytoplankton analysis. UNESCO, Paris, 37–39.

Danielson, S., Eisner, L., Weingartner, T., Aagaard, K., 2011. Thermal and haline variability over the central Bering Sea shelf: Seasonal and interannual perspectives. Cont. Shelf Res., 31, 539–554.

Danielson, S.L., Eisner, L., Ladd, C., Mordy, C., Sousa, L., Weingartner, T.J., 2017. A comparison between late summer 2012 and 2013 water mass, macronutrients, and phytoplankton standing crops in the northern Bering and Chukchi. Deep-Sea Res. II, 135, 7–26.

Duffy-Anderson, J.T., Stabeno, P., Andrews III, A.G, Cieciel, K., Deary, A., Farley, E., Fugate, C., Harpold, C., Heintz, R., Kimmel, D., Kuletz, K., Lamb, J., Paquin, M., Porter, S., Rogers, L., Spear, A., Yasumiishi, E., 2019. Responses of the Northern Bering Sea and southeastern Bering Sea pelagic ecosystems following record-breaking low winter sea ice. Geophys. Res. Let. 46, 9833–9842.

Field, J.G., Clarke, K.R., Warwick, R.M., 1982. A practical strategy for analyzing

490 multispecies distribution patterns. Mar. Ecol. Prog. Ser. 8, 37–52.
491 Frey, K.E., Comiso, J.C., Cooper, L.W., Grebmeier, J.M., Stock, L.V., 2018. Arctic ocean
492 primary productivity: the response of marine algae to climate warming and
493 sea ice decline. In: Arctic Report Card. Arctic Region 2018,
494 ⟨http://www.arctic.noaa.gov/ reportcard⟩.
495 Fujiwara, A., Hirawake, T., Suzuki, K., Eisner, L., Imai, I., Nishino, S., Kikuchi, T., Saitoh,
496 S.-I., 2016. Influence of timing of sea ice retreat on phytoplankton size
497 during marginal ice zone bloom period on the Chukchi and Bering shelves.
498 Biogeosciences 13, 115–131.
499 Fukai, Y., Matsuno, K., Fujiwara, A., Yamaguchi, A., 2019. The community composition
500 of diatom resting stages in sediments of the northern Bering Sea in 2017
501 and 2018: the relationship to the interannual changes in the extent of the sea
502 ice. Polar Biol. 42, 1915–1922.
503 Giesbrecht, K.E., D.E. Varela, J. Wiktor, J.M. Grebmeier, B. Kelly, J.E. Long, 2019. A
504 decade of summertime measurements of phytoplankton biomass,
505 productivity and assemblage composition in the Pacific Arctic Region from
506 2006 to 2016. Deep-Sea Res. II 162, 93–113.
507 Grebmeier, J.M., McRoy, C.P., Feder, H.M., 1988. Pelagic-benthic coupling on the shelf
508 of the northern Bering and Chukchi Seas. I. Food supply source and benthic
509 biomass. Mar. Ecol. Prog. Ser. 48, 57−67.
510 Grebmeier, J.M., Bluhm, B.A., Cooper, L.W., Danielson, S.L., Arrigo, K.R., Blanchard,
511 A.L., Clarke, J.T., Day, R.H., Frey, K.E., Gradiner, R.R., Kędra, M., Konar,
512 B., Kuletz, K.J., Lee, S.H., Lovvorn, J.R., Norcross, B.L., Okkonen, S.R.,
513 2015. Ecosystem characteristics and processes facilitating persistent
514 macrobenthic biomass hotspots and associated benthivory in the Pacific

Arctic. Prog. Oceanogr. 136, 92–114.

Grebmeier, J.M., Moore, S.E., Cooper, L.W., Frey, K.E., 2019. The Distributed Biological Observatory: A change detection array in the Pacific Arctic – An introduction. Deep-Sea Res. II 162, 1–7.

Harada, N., Sato, M., Oguri, K., Hagino, K., Okazaki, Y., Katsuki, K., Tsuji, Y., Shin, K.-H., Tadai, O., Saitoh, S.-I., Narita, H., Konno, S., Jordan, R.W., Shiraiwa, Y., Grebmeier, J., 2012. Enhancement of coccolithophorid blooms in the Bering Sea by recent environmental changes. Global Biogeochem. Cycles 26, GB2036.

Hasle, G.R., Syvertsen, E.E., 1997. Marine diatoms. In: Tomas, C.R. (Ed). Identifying marine phytoplankton. Academic Press, San Diego, 5–385

Hoppenrath, M., Elbrächter, M., Drebes, G., 2009. Marine phytoplankton: selected microphytoplankton species from the North Sea around Helgoland and Sylt., Schweizerbart Science Publishers.

Hunt, G.L., Stabeno, P., Walters, G., Sinclair, E., Brodeur, R.D., Napp, J.M., Bond, N.A., 2002. Climate change and control of the southeastern Bering Sea pelagic ecosystem. Deep-Sea Res. II 49, 5821–5853.

Huntington, H.P., Danielson, S.L., Wiese, F.K., Baker, M.R., Boveng, P., Citta, J.J., De Robertis, A., Dickson, D.M.S., Farley, E.V., George, J.C., Iken, K., Kimmel, D.G., Kuletz, K., Ladd, C., Levine, R., Quakenbush, L., Stabeno, P., Stafford, K.M., Stockwell, D., Wilson C., 2020. Evidence suggests potential transformation of the Pacific Arctic ecosystem is underway. Nat. Clim. Change 10, 342–349.

Hydes, D.J., Aoyama, M., Aminot, A., Bakker, K., Becker, S., Coverly, S., Daniel, A., Dickson, A.G., Grosso, O., Kerouel, R., van Ooijen, J., Sato, K., Tanhua, T.,

Woodward, E.M.S., Zhang, J.Z., 2010. Determination of dissolved nutrients (N, P, Si) in seawater with high precision and inter-comparability using gas-segmented continuous flow analysers. In: Hood, E.M., Sabine, C.L., Sloyan, B.M. (Eds.). The GO-SHIP Repeat Hydrography Manual: A Collection of Expert Reports and Guidelines. IOCCP report number 14, ICPO publication series number 134, U.N. Educ. Sci. and Cult. Organ. Intergov. Oceanotr. Comm., Paris, 1–88.

Iida, T., Saitoh, S.I., Miyamura, T., Toratani, M., Fukushima, H., Shiga, N., 2002. Temporal and spatial variability of coccolithophore blooms in the eastern Bering Sea, 1998-2001. Prog. Oceanogr. 55, 165–175.

Justic, D., Rabalais, N.N., Turner R.E., Dortch, Q., 1995. Changes in nutrient structure of river-dominated coastal waters: Stoichiometric nutrient balance and its consequences. Estuar. Coast. Shelf Sci. 40, 339–356.

Matsuno, K., Ichinomiya, M., Yamaguchi, A., Imai, I., Kikuchi, T., 2014. Horizontal distribution of microprotist community structure in the western Arctic Ocean during late summer and early fall of 2010. Polar Biol. 37, 1185–1195.

Neeley, A.R., Harris, L.A., Frey, K.E., 2018. Unraveling phytoplankton community dynamics in the northern Chukchi Sea under sea-ice-covered and sea-ice-free conditions. Geophys Res. Let. 45, 7663–7671.

Parsons, T.R., Harrison, P.J., Waters, R., 1978. An experimental simulation of changes in diatom and flagellate blooms. J. Exp. Biol. Ecol. 32, 285–294.

Quinn, G.P., Keough, M.J., 2002. Experimental Design and Data Analysis for Biologists. Cambridge University Press, New York.

Sergeeva, V.M., Sukhanova, I.N., Flint, M.V., Pautova, L.A., Grebmeier, J.M., Cooper, L.W., 2010. Phytoplankton community in the western Arctic in July–August

2003. Oceanology 50, 184–197.

Shannon, C.E., Weaver, W., 1949. The mathematical theory of communication. The University of Illinois Press, Urbana.

Springer, A.M., McRoy, C.P., 1993. The paradox of pelagic food webs in the northern Bering Sea III. Patterns of primary production. Cont. Shelf. Res. 13, 575–599.

Springer, A.M., McRoy, C.P., Flint, M.V., 1996. The Bering Sea Green Belt: shelf-edge processes and ecosystem production. Fish. Oceanogr. 5(3/4), 205–223.

Stockwell, D.A., Whitledge, T.E., Zeeman, S.I., Coyle, K.O., Napp, J.M., Brodeur, R.D., Pinckuk, A.I., Hunt, G.L. 2001. Anomalous conditions in the south-eastern Bering Sea, 1997: nutrients, phytoplankton and zooplankton. Fish. Oceanogr. 10, 99–116.

Taniguchi, A., Saito, K., Koyama, A., Fukuchi, M., 1976. Phytoplankton communities in the Bering Sea and adjacent seas I. Communities in early warming season in southern areas. J. Oceanogr. Soc. Jpn. 32, 99–106.

von Quillfeldt, C.H., 2000. Common diatom species in Arctic spring blooms: Their distribution and abundance. Bot. Mar. 43, 499–516.

von Quillfeldt, C.H., Ambrose Jr., W.G., Clough, L.M., 2003. High number of diatom species in first-year ice from the Chukchi Sea. Polar Biol. 26, 806–818.

584

585 **Figure legends**

586 **Fig. 1.** Location of stations in the northern Bering Sea from July 9–21, 2017 and
587 July 2–12, 2018. The numbers indicate the station ID. The open and solid
588 circles indicate stations with hydrographic observations only taken by CTD
589 and those with water sampling and hydrographic observations, respectively.

590 **Fig. 2.** Cross-sectional distributions of the temperature, salinity, and fluorescence in
591 the northern Bering Sea in 2017 (upper) and 2018 (lower).

592 **Fig. 3.** T-S diagrams of all the stations in 2017 (upper) and 2018 (lower). Note that
593 the symbols of the stations vary with the geographical location.

594 **Fig. 4.** Spatial distribution of water masses as defined by Danielson et al. (2017).
595 BCSW: Bering-Chukchi Summer Water, ACW: Alaskan Coastal Water, MW:
596 Melting Water, and BCWW: Bering-Chukchi Winter Water.

597 **Fig. 5.** Cross-sectional distributions of nutrient (NO_2-N + NO_3-N, NH_4-N, PO_4-P,
598 and Si $(OH)_4$) concentrations in the northern Bering Sea in 2017 (upper) and
599 2018 (lower).

600 **Fig. 6.** Horizontal distribution of the average phytoplankton cell density in 2017
601 (left) and 2018 (right). The circles indicate the mean cell density in the water
602 column.

603 **Fig. 7.** (a) Results of the cluster analysis based on the phytoplankton cell density
604 found by Bray-Curtis similarity. (b) Species composition and cell density of
605 each group. (c) Spatial distribution of the phytoplankton community in the
606 northern Bering Sea during the summers of 2017 (left) and 2018 (right). (d)
607 Nonmetric multidimensional scaling plots of the four groups, with *arrows*
608 and *percentages* indicating the directions of the environmental parameters

609 and the coefficient of determination (r^2), respectively. *Obs. date*: observation
610 date, *Si*: silicate, *Sal*: salinity, *N*: nitrate and nitrite, *TSR*: the timing of sea ice
611 retreat, *Fluor*: fluorescence, and *Dep*: sampling depth.
612
613 **Appendix Fig 1.** Relationship between the chlorophyll *a* concentration and the
614 fluorescence.
615 **Appendix Fig 2.** Spatial distribution of the phytoplankton communities in each water
616 mass (the BCSW (a) and the ACW (b)) by cluster analyses. The cluster
617 analyses were conducted in each water mass independently. White boxes
618 indicated water masses that were not the focus of this analysis. Color codes
619 for the communities were shown different groups analyzed by the cluster
620 analysis.
621 **Appendix Fig 3.** Spatial distribution of the phytoplankton communities in each year.
622 Cluster analyses were conducted in each year independently. Color codes for
623 the communities were shown different groups analyzed by the cluster
624 analysis.
625

626 Table 1. List of phytoplankton species identified in the water samples that were collected
627 from the northern Bering Sea and Bering Strait in July 2017 and 2018.

Class Bacillariophyceae		
Order Centrales		
Actinocyclus spp.	*C. furcellatus*	*Ditylum* spp.
Actinoptychus spp.	*C. gelidus*	*Eucampia* spp.
Attheya spp.	*C. laciniosus*	*Lauderia annulata*
Bacterosira bathyomphala	*C. lorenzianus*	*Leptocylindrus danicus*
Chaetoceros conturtus	*C. mitra*	*L. minimus*
C. convolutus/concavicornis/borealis	*C. subtilis*	*Odontella aurita*
C. curvicetus	*C. teres*	*Paralia sulcata*
C. danicus	*Chaetoceros* spp.	*Rhizosolenia* spp.
C. debilis	*Corethron hystrix*	*Skeletonema* spp.
C. decipiens	*Coscinodiscus* spp.	*Stephanopyxis turris*
C. diadema	*Detonula pumuila*	*Thalassiosira* spp.
C. didymus	*Dactyliosolen fragilissimus*	Other centric diatoms
Order Pennales		
Asteroplanus karianus	*Pauelia taeniata*	*Navicula* spp.
Asterionellopsis glacialis	*Pleurosigma* spp.	*Nitzschia* spp.
Cylindrotheca closterium	*Pseudo-nitzschia* spp.	Other pennate diatoms
Thalassionema nitzschioides	*Fragilariopsis* spp.	
Class Dinophyceae		
Alexandrium spp.	*Protoperidinium* spp.	*Dinophysis norvegica*
Ceratium spp.	*Heterocapsa triquetra*	*Dinophysis rudgei*
Prorocentrum triestinum	*Dinophysis acuta*	Other dinofalagellates

628

629

630 Table 2. Comparison of phytoplankton species in the phytoplankton community groups
631 (A–D). The values are given as the mean cell density (× 10^3 cells L^{-1}) and standard
632 deviation in each group. The numbers in parentheses indicate the number of stations. The
633 differences among the phytoplankton communities were evaluated by a one-way ANOVA
634 and a Tukey-Kramer test. Any groups not connected by the underlines are significantly
635 different (*: $p < 0.05$, **: $p < 0.01$, and ***: $p < 0.005$).
636

Species	Group name				One-way ANOVA	Tukey-Kramer test
	A (5)	B (74)	C (41)	D (21)		
C. convolutus/concavicornis/borealis	4.49 ± 6.47	3.56 ± 7.79	4.37 ± 9.50	0.26 ± 1.01	NS	
C. debilis	–	16.45 ± 42.68	0.20 ± 1.05	–	*	Not detected
C. diadema	0.65 ± 1.29	3.35 ± 4.73	0.06 ± 0.20	0.01 ± 0.02	***	D C A B
C. furcellatus	–	49.95 ± 118.66	–	–	**	Not detected
C. gelidus	31.28 ± 44.80	65.46 ± 114.33	0.02 ± 0.06	0.12 ± 0.33	***	C D A B
Chaetoceros spp.	2.22 ± 2.81	13.94 ± 20.48	0.84 ± 2.91	0.50 ± 1.36	***	D C A B
Leptocylindrus danicus	–	15.43 ± 30.69	3.08 ± 10.43	21.01 ± 89.63	NS	
Cylindrotheca closterium	0.05 ± 0.05	1.09 ± 1.03	1.79 ± 1.60	0.15 ± 0.27	***	A D B C
Thalassionema nitzschioides	0.21 ± 0.28	0.68 ± 1.05	7.51 ± 15.35	0.47 ± 0.95	***	A D B C
Pseudo-nitzschia spp.	–	5.23 ± 12.90	1.45 ± 4.94	0.08 ± 0.34	NS	
Fragilariopsis spp.	0.02 ± 0.04	2.92 ± 10.65	0.41 ± 1.09	0.05 ± 0.21	NS	

637

Table 3. Hydrographic environmental factors among the phytoplankton communities (A–D). The values are given as the average and standard deviation of each factor. The numbers in parentheses indicate the number of stations. The differences among the phytoplankton communities were evaluated by a one-way ANOVA and a Tukey-Kramer test. Any groups not connected by the underlines are significantly different (*: $p < 0.05$, **: $p < 0.01$, and ***: $p < 0.005$).

Factors	Group name				One-way ANOVA	Tukey-Kramer test
	A (5)	B (74)	C (41)	D (21)		
Temperature	1.97 ± 3.29	3.56 ± 1.66	2.89 ± 2.49	6.21 ± 2.78	**	A C B D
Fluorescence	0.54 ± 0.56	0.75 ± 0.53	0.44 ± 0.17	0.20 ± 0.13	***	D C A B
Salinity	32.00 ± 0.32	32.49 ± 0.41	32.10 ± 0.87	31.58 ± 0.36	***	D A C B
NO_2+NO_3	5.68 ± 6.55	9.34 ± 6.38	7.88 ± 6.29	0.96 ± 1.01	**	D A C B
PO_4-P	1.18 ± 0.65	1.35 ± 0.83	1.42 ± 0.39	0.80 ± 0.32	NS	
NH_4-N	1.11 ± 1.43	0.78 ± 0.48	0.84 ± 0.61	0.18 ± 0.13	*	D B C A
Si $(OH)_4$	29.48 ± 40.68	25.01 ± 13.25	19.10 ± 12.29	8.60 ± 7.69	*	D C B A
DIN	6.79 ± 7.95	10.41 ± 6.76	10.59 ± 13.33	1.13 ± 1.11	NS	
N/P	4.30 ± 3.34	7.24 ± 3.46	6.94 ± 9.78	1.28 ± 1.02	NS	
TSR	91.00 ± 8.22	115.28 ± 14.44	107.78 ± 11.67	99.38 ± 15.44	***	A D C B

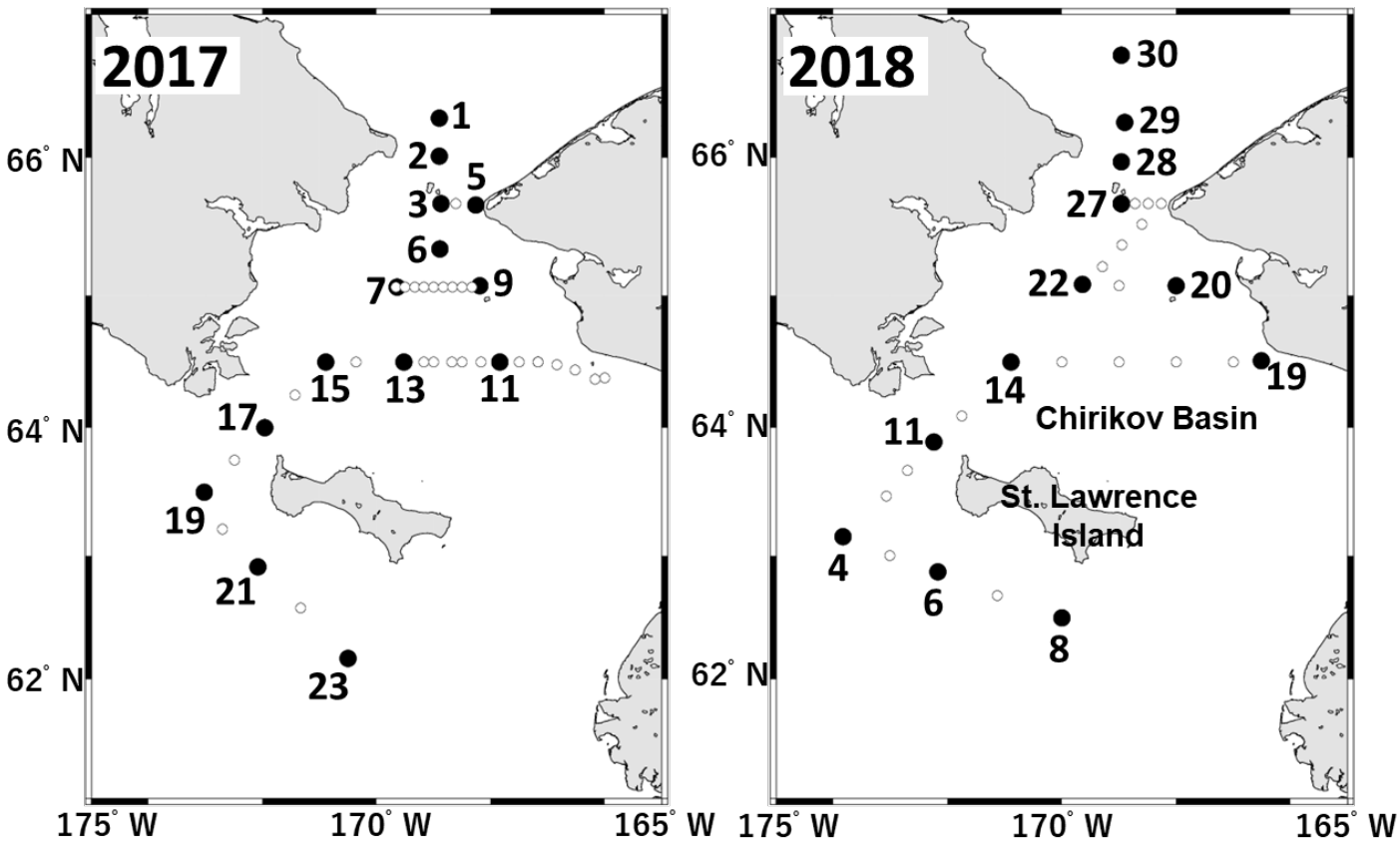

Fig. 1. Location of stations in the northern Bering Sea from July 9–21, 2017 and July 2–12, 2018. The numbers indicate the station ID. The open and solid circles indicate stations with hydrographic observations only taken by CTD and those with water sampling and hydrographic observations, respectively.

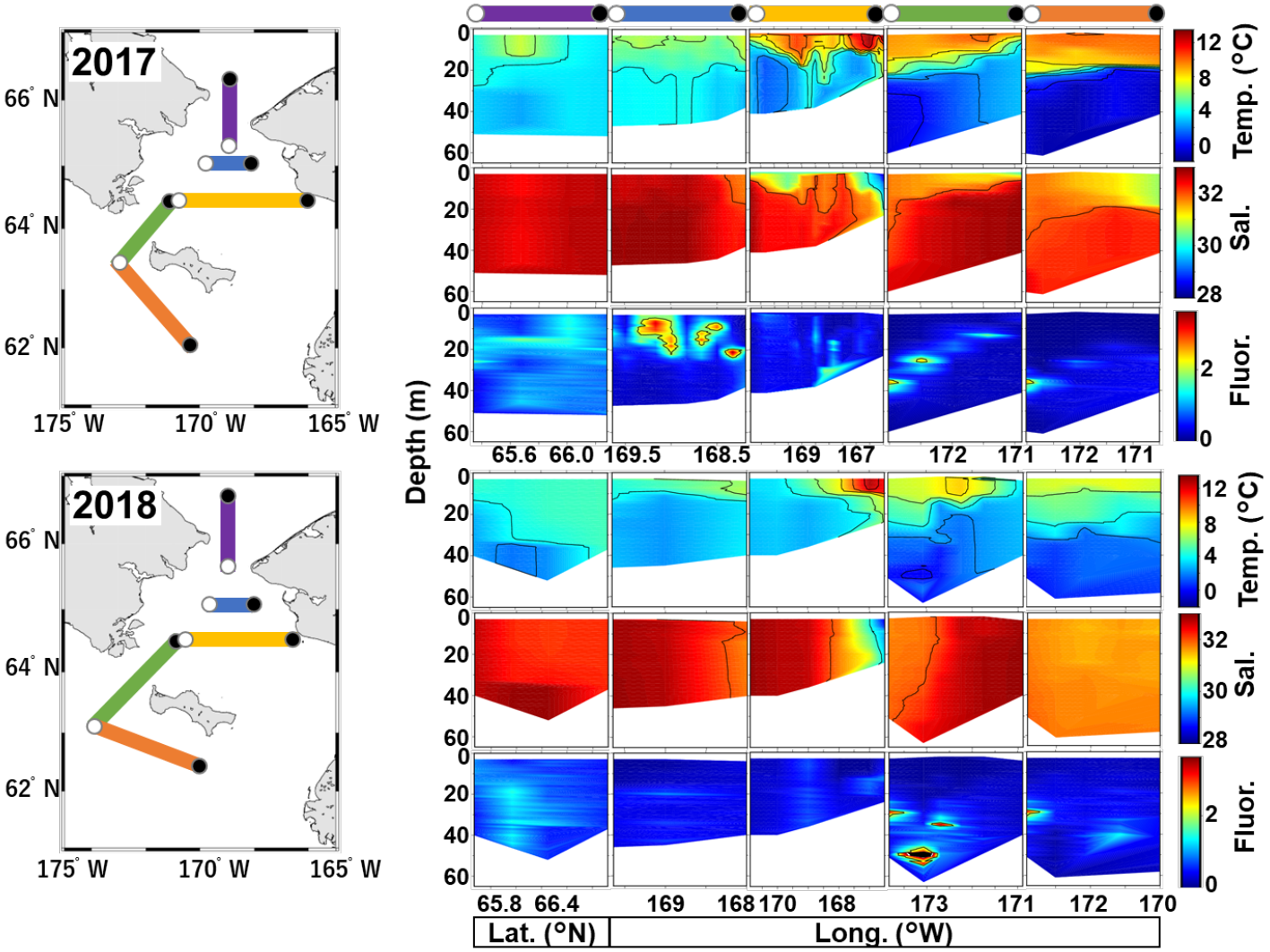

Fig. 2. Cross-sectional distributions of the temperature, salinity, and fluorescence in the northern Bering Sea in 2017 (upper) and 2018 (lower).

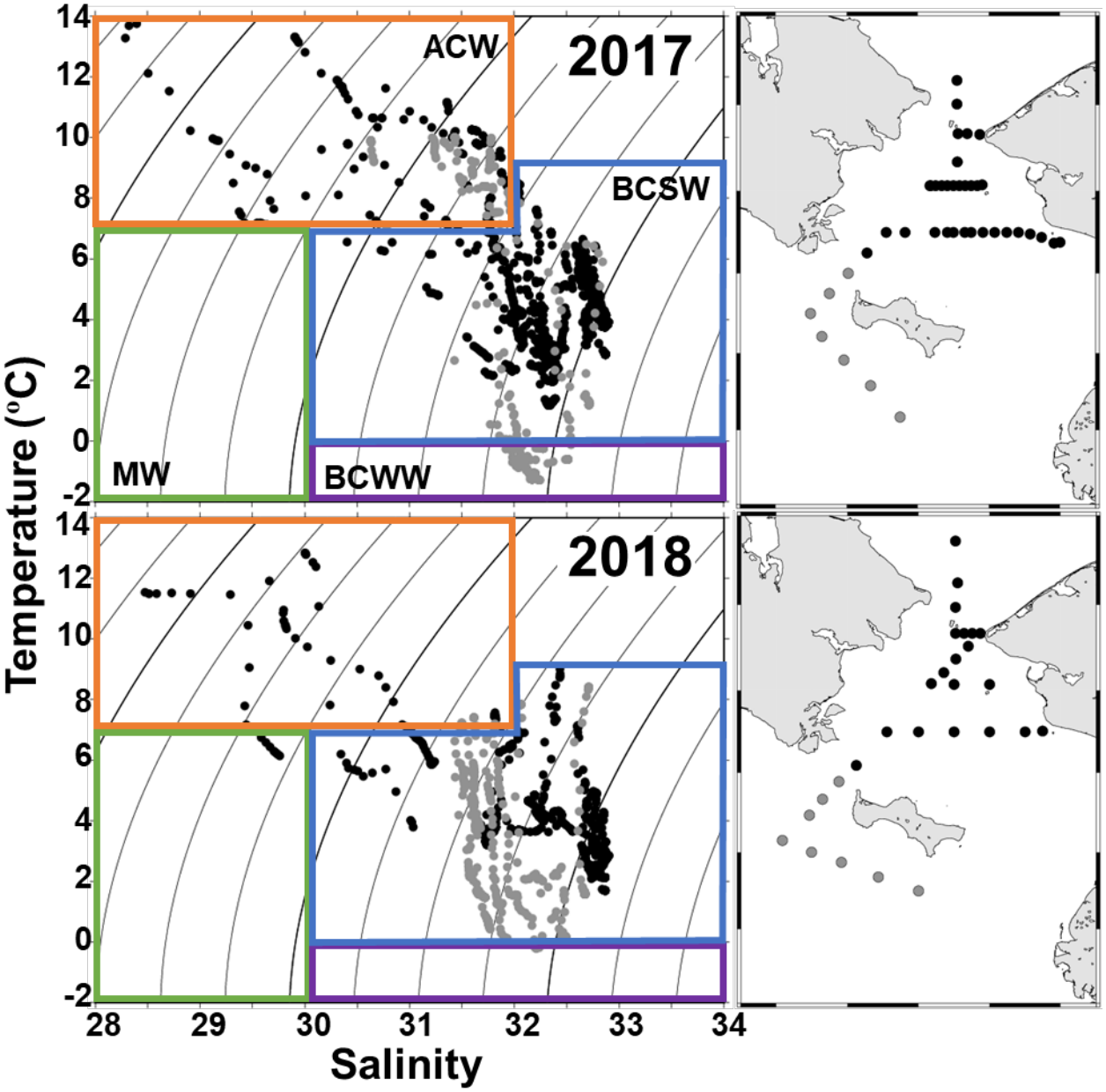

Fig. 3. T-S diagrams of all the stations in 2017 (upper) and 2018 (lower). Note that the symbols of the stations vary with the geographical location.

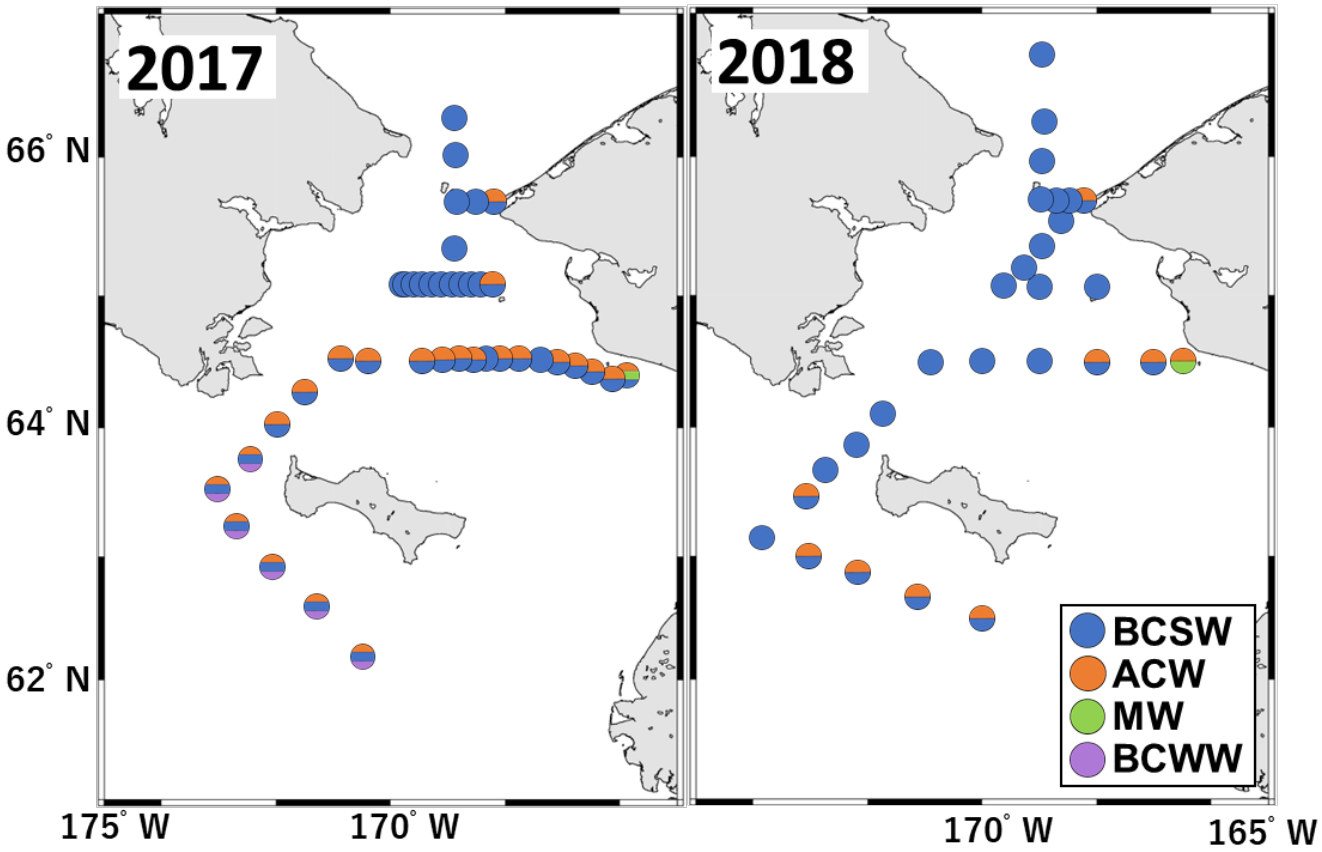

Fig. 4. Spatial distribution of water masses as defined by Danielson et al. (2017). BCSW: Bering-Chukchi Summer Water, ACW: Alaskan Coastal Water, MW: Melting Water, and BCWW: Bering-Chukchi Winter Water.

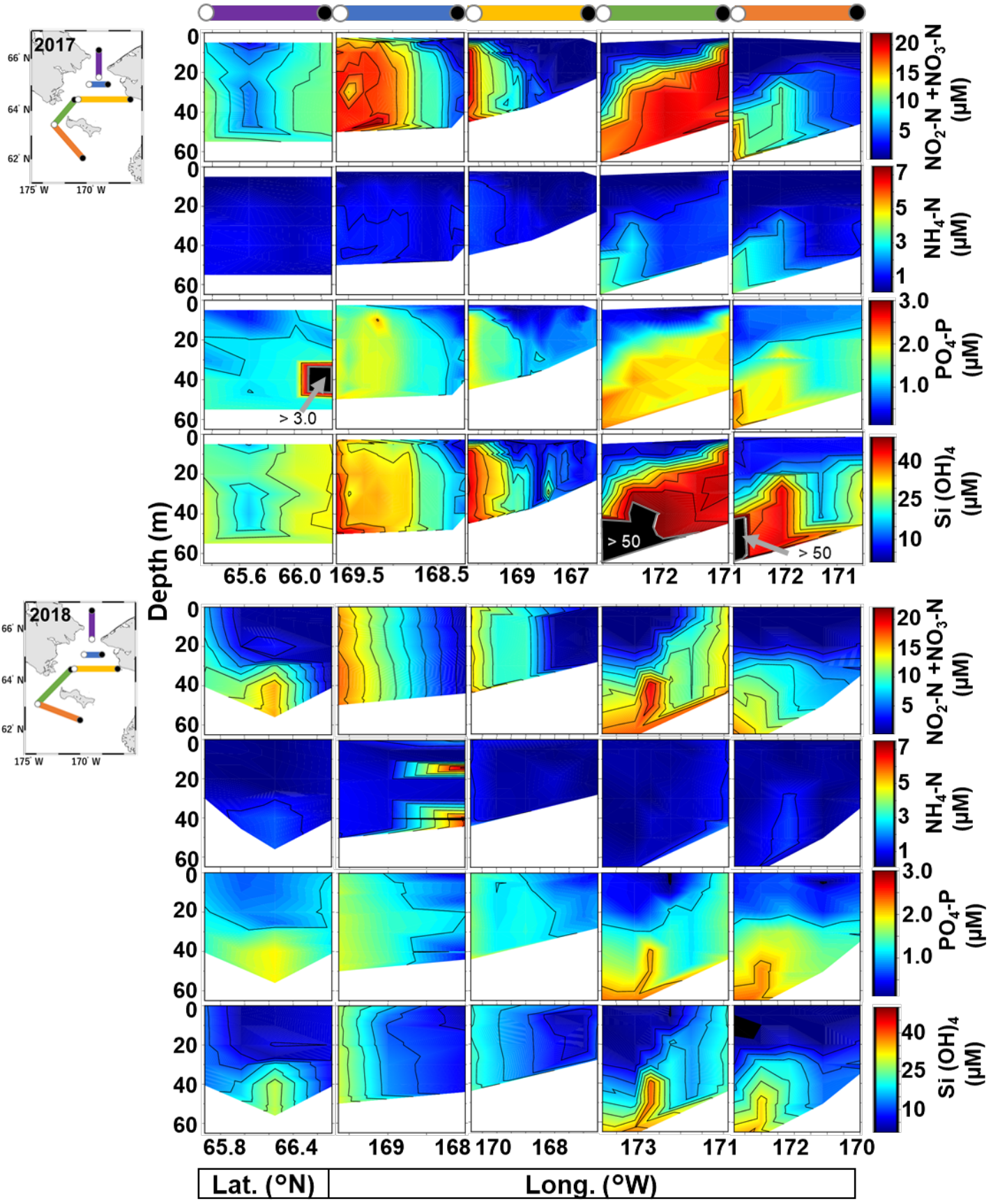

Fig. 5. Cross-sectional distributions of nutrient (NO_2-N + NO_3-N, NH_4-N, PO_4-P, and Si $(OH)_4$) concentrations in the northern Bering Sea in 2017 (upper) and 2018 (lower).

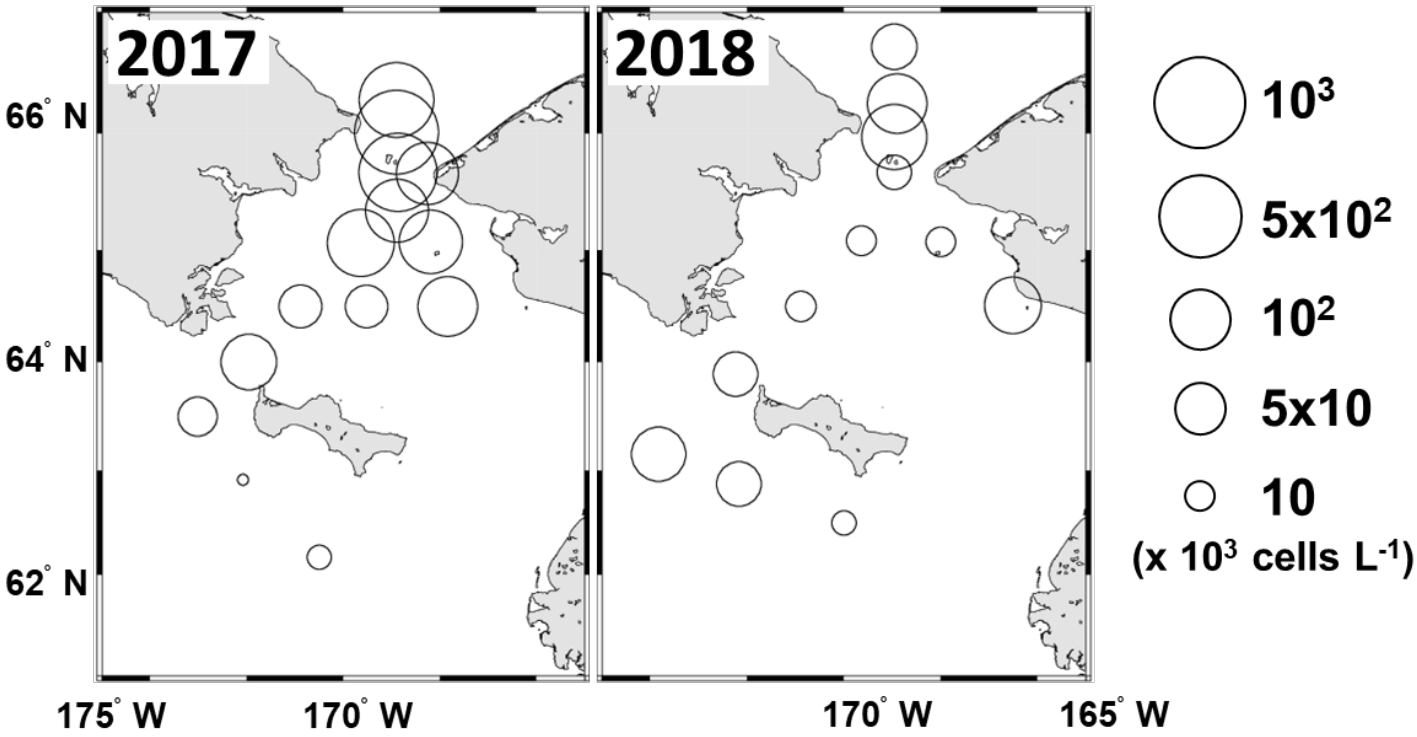

Fig. 6. Horizontal distribution of the average phytoplankton cell density in 2017 (left) and 2018 (right). The circles indicate the mean cell density in the water column.

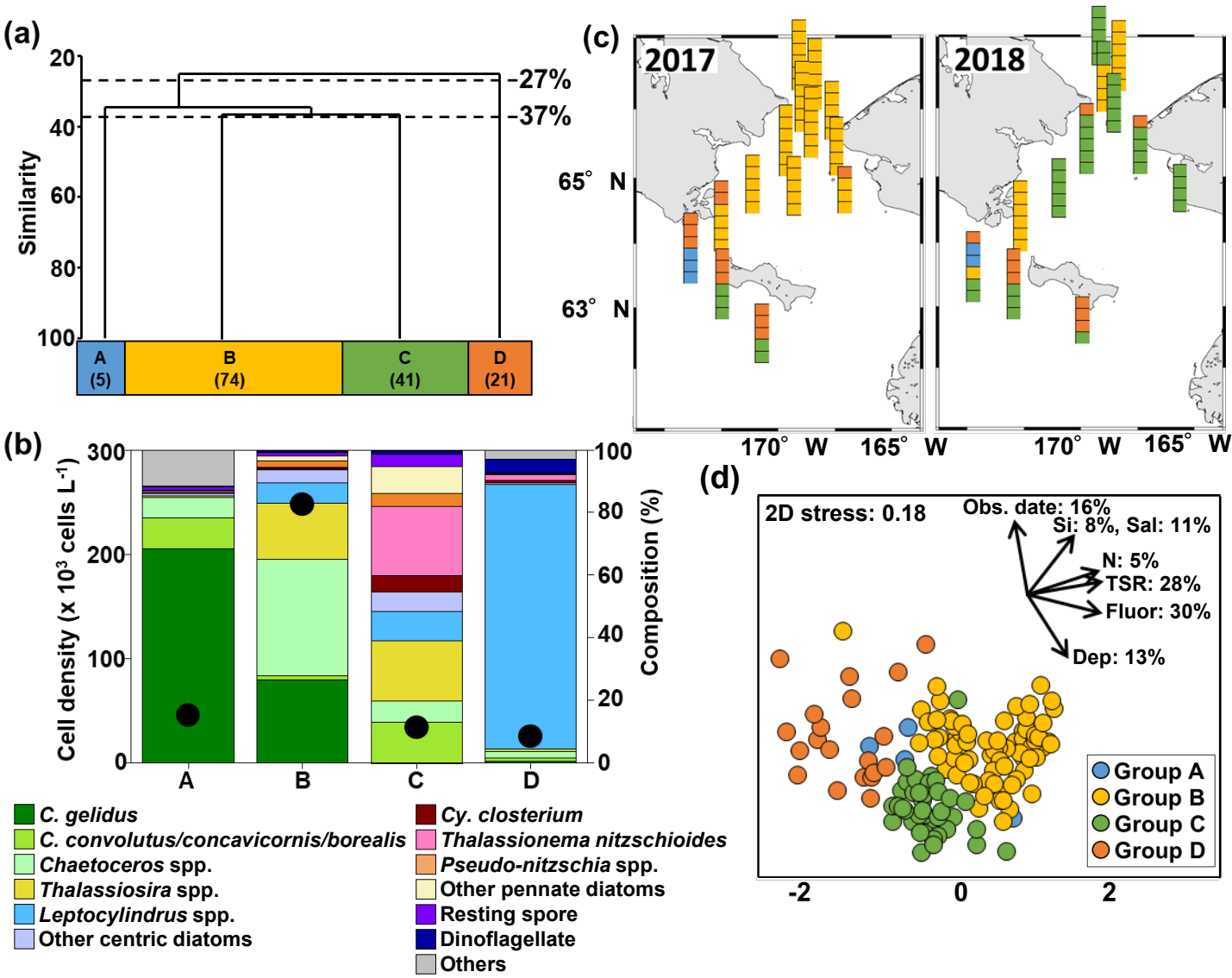

Fig. 7. (a) Results of the cluster analysis based on the phytoplankton cell density found by Bray-Curtis similarity. (b) Species composition and cell density of each group. (c) Spatial distribution of the phytoplankton community in the northern Bering Sea during the summers of 2017 (left) and 2018 (right). (d) Nonmetric multidimensional scaling plots of the four groups, with *arrows* and *percentages* indicating the directions of the environmental parameters and the coefficient of determination (r^2), respectively. *Obs. date*: observation date, *Si*: silicate, *Sal*: salinity, *N*: nitrate and nitrite, *TSR*: the timing of sea ice retreat, *Fluor*: fluorescence, and *Dep*: sampling depth.

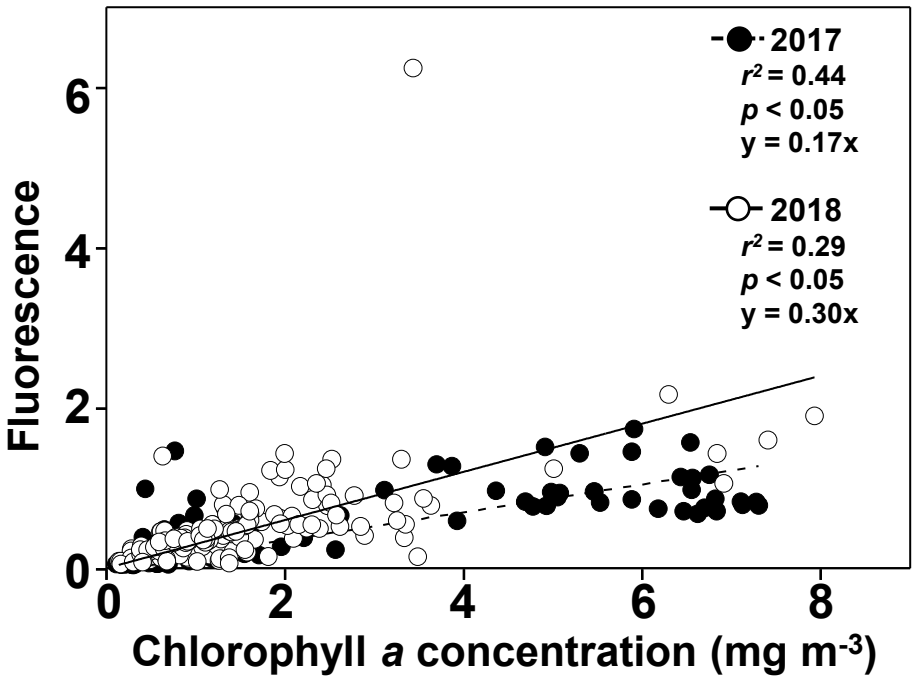

Appendix Fig 1. Relationship between the chlorophyll *a* concentration and the fluorescence.

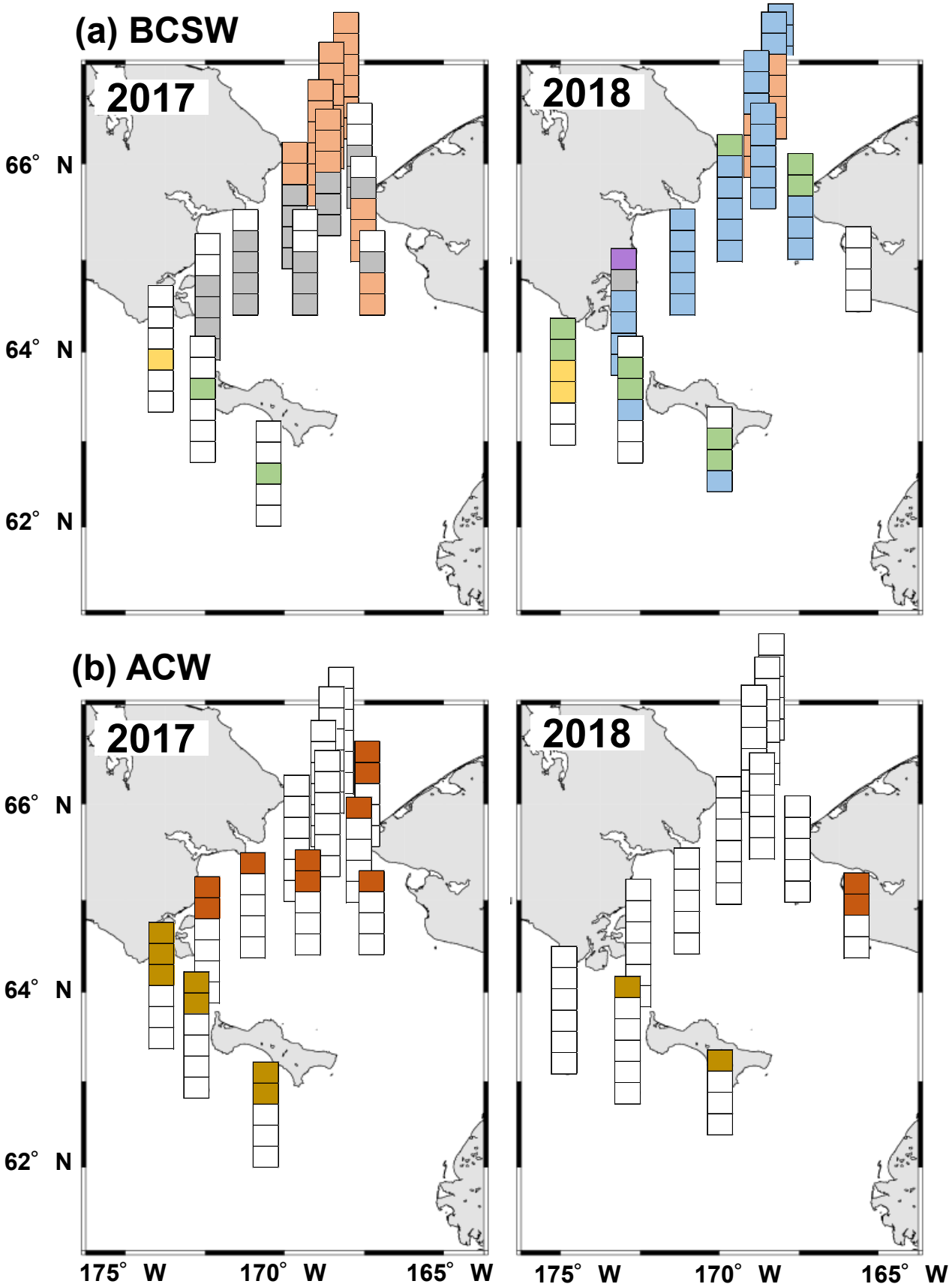

Appendix Fig 2. Spatial distribution of the phytoplankton communities in each water mass (the BCSW (a) and the ACW (b)) by cluster analyses. The cluster analyses were conducted in each water mass independently. White boxes indicated water masses that were not the focus of this analysis. Color codes for the communities were shown different groups analyzed by the cluster analysis.

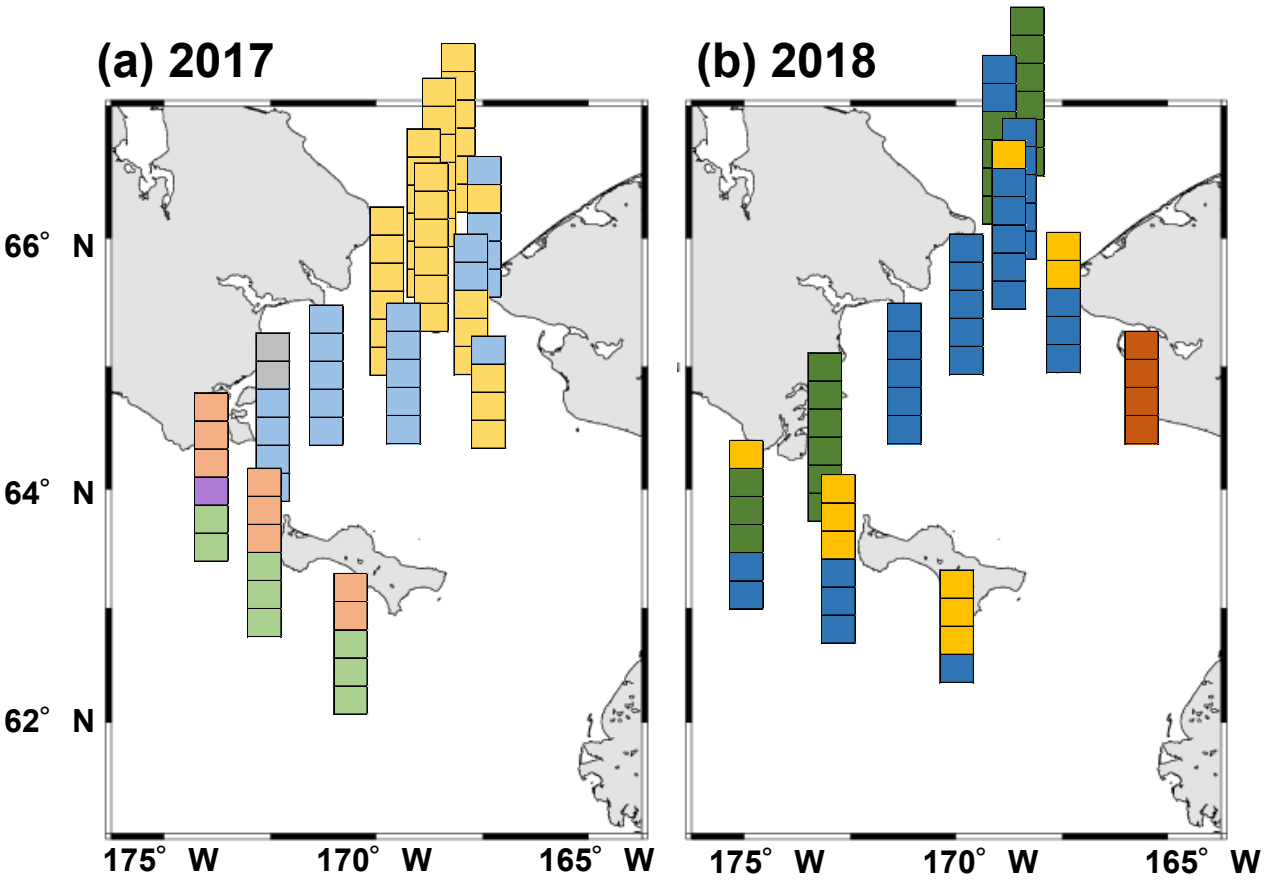

Appendix Fig 3. Spatial distribution of the phytoplankton communities in each year. Cluster analyses were conducted in each year independently. Color codes for the communities were shown different groups analyzed by the cluster analysis.